THE ASTROPHYSICAL JOURNAL, 416:36–50, 1993 October 10

THE DYNAMICS OF THE GALAXY CLUSTER ABELL 2634

J. PINKNEY, G. RHEE, AND J. O. BURNS
Department of Astronomy, Box 30001/Department 4500, New Mexico State University, Las Cruces, NM 88003-0001
J. M. HILL
Steward Observatory, University of Arizona, Tucson, AZ 85721
W. OEGERLE
Space Telescope Science Institute, 3700 San Martin Drive, Baltimore, MD 21218
D. BATUSKI
Department of Physics and Astronomy, University of Maine, Orono, ME 04469
AND
P. HINTZEN
Physics Department, University of Nevada, 4505 South Maryland Parkway, Las Vegas, NV 89154
Received 1992 August 27; accepted 1993 February 24

ABSTRACT

We have collected a large sample of galaxy velocities for the nearby, rich cluster of galaxies Abell 2634, which contains the prototypical wide-angle tailed (WAT) radio source 3C 465 associated with the central cD galaxy. Robust indicators of location (i.e., velocity mean) and scale (velocity dispersion) and their confidence intervals are used to determine the velocity structure of the cluster. We find a cD peculiar radial velocity of -219 ± 98 km s^{-1}. The Dressler-Shectman δ-test reveals significant deviations in the local dynamics on the east side of the cluster, probably due to subcluster contamination. The velocity distribution is Gaussian except for a few outliers, where the velocity outliers tend to be spatial outliers. We consider ways in which a cluster-subcluster merger could lead to the observed peculiar motion. We conclude that A2634 is an unrelaxed cluster whose X-ray and radio source structures have resulted from the turbulent gas motion of an ongoing merger.

Subject headings: galaxies: clusters: individual (Abell 2634) — galaxies: distances and redshifts — galaxies: elliptical and lenticular, cD

1. INTRODUCTION

Abell 2634 is a cluster of galaxies with an abundance of interesting features. It is a Rood-Sastry type cD cluster (Sastry & Rood 1971) of richness class 1, and distance class 1 (Abell 1958). Its 13.9 mag first-ranked galaxy, NGC 7720, was classified as cD by Matthews, Morgan, & Schmidt (1964) but has been classified as D by Dressler (1980). NGC 7720 is centrally located in the cluster and contains a companion, NGC 7720A, projected about 12″ (7.2 h_{75}^{-1} kpc) away from the cD nucleus. Scott, Robertson, & Tarenghi (1977) and Jenner (1974) both measured a velocity difference of about 1000 km s^{-1} for NGC 7720A, thus calling into question its association with NGC 7720. High signal-to-noise spectroscopy by De Robertis & Yee (1990) strongly suggests nuclear activity slightly offset to the south of the continuum centroid of NGC 7720. They also find distorted inner contours and a centroid shift for the outer contours relative to the inner ones.

Furthermore, the A2634 field has substantial diffuse X-ray emission (Eilek et al. 1984). The cD nucleus coincides with the X-ray emission peak, but there is no evidence of a cooling inflow. This is unusual since recent analyses by Edge & Stewart (1991) suggest that up to 90% of clusters with dominant galaxies have cooling flows.

It was recently found that secondary distance indicators give a very different distance for A2634 than the Hubble law, suggesting that the cluster may have a peculiar motion as large as -3400 km s^{-1} relative to the Hubble flow (Lucey et al. 1991). In addition, A2666 is only 2°.8 to the east of A2634 and differs by ≈ 1000 km s^{-1} in redshift; the two may be associated in a supercluster (Batuski & Burns 1985).

Finally, one of A2634's most intriguing features is the prototype wide-angle tailed (WAT) radio source, 3C 465, whose core also coincides with NGC 7720 (Griffen 1963). Most of the above features of A2634 can play a role in the question which instigated this project: which factors determine the structure and creation of the radio source 3C 465? The defining characteristics of WAT radio sources are described in O'Donoghue, Owen, & Eilek (1990). The C-shape formed by the two bent tails (see Fig. 4) has suggested to some that WATs are the slower, more massive analog of the narrow-angle tail (NAT) phenomenon (see O'Dea & Owen 1985), where motion of the galaxy through the intracluster medium (ICM) bends back the tails via ram pressure (Jones & Owen 1979). The tails of 3C 465 are quite symmetrically bent, forming an $\approx 90°$ angle with each other. Eilek et al. (1984) looked carefully at the physics involved in bending and disrupting the jets at the hot spots and found that galaxy velocities of order 1000 km s^{-1} with respect to the ICM would be required for the ram pressure model. O'Donoghue, Eilek, & Owen (1992) have recently reexamined the bending phenomenon and found that if another mechanism can be employed to disrupt the jets, such as a pressure transition at the ISM/ICM interface (Burns, Norman, & Clarke 1991), lower velocities would be required to shape the tails. O'Donoghue found for tails that emit without in situ energization (the *adiabatic* model), the tails will bend by ram pressure even with low galaxy velocities (100 km s^{-1} was used). Their *kinetic* model, which is the opposite extreme where all

energization occurs by in situ processes, does not allow the ram pressure bending. The true case is probably somewhere between these two models, so a lower limit on the required velocity is uncertain.

The motion of the host galaxy through a stationary ICM appears to be too simplistic a model to explain the structures found. Not all of the WATs in the O'Donoghue et al. (1990) sample show tails bent as symmetrically as 3C 465, and one (Abell 690) even shows the two tails bending in opposite directions. If ram pressure is the bending agent, the twisting of individual tails suggests an ICM with a complex velocity field.

The simple ram pressure model is also problematic because there are several reasons to expect central dominant galaxies (CDGs), like those containing WATs, to be at rest in their cluster. First, CDGs are repeatedly found near the optical and X-ray cluster centroids. Second, the lack of tidal truncation of extended cD envelopes places limitations on the velocity of the CDGs through the cluster center (Merritt 1984).

Early studies of CDG peculiar motions (i.e., the difference between the CDG radial velocity and the cluster velocity centroid) reported results consistent with a nonmoving CDG and indicated upper limits for their true velocities around 300 km s^{-1} (e.g., the 28 cD, D, and dumbell clusters studied by Quintana & Lawrie 1982). Larger redshift samples have subsequently been completed so that there is a growing sample of CDGs with a significant peculiar motion (Sharples, Ellis, & Gray 1988; Hill et al. 1988; Oegerle & Hill 1992). Malumuth et al. (1992) review 22 clusters with more than 20 measured velocities and find that their radial peculiar motions tend to be within 30% of the cluster velocity dispersion. However, still more recent studies have revealed that apparent peculiar motions can result from subcluster contamination of the cluster centroid (Beers et al. 1991; Teague, Carter, & Gray 1990).

Previous redshift studies of Abell 2634 have utilized small sample sizes. Scott et al. (1977) had $N = 17$, Bothun & Schombert (1988) had $N = 25$, Zabludoff, Huchra, & Geller (1990) had $N = 29$, and Lucey et al. (1991) had $N = 25$. Thus, it was difficult to measure any cD peculiar motions given the small number statistics. The recent development of fiber-fed multiple aperture spectrographs has made it practical to measure the velocities of hundreds of cluster members with sufficient accuracy to reliably detect cD peculiar radial velocities of 300 km s^{-1} or less.

In this paper, we have set out to investigate the dynamics of A2634 to help us understand the formation of the enigmatic WAT, 3C 465. We wish to substantially increase the velocity sample size in order to add conclusive dynamical information to available radio and X-ray data. In particular, we want to know if the cD is moving within the cluster and if the cluster is dynamically evolved. The paper will proceed as follows. Section 2 will describe our multifiber observations and reductions, including velocity errors. Section 3 will present the velocity data. Section 4 will describe our extensive analysis of our A2634 velocity sample including its fairness, the cD peculiar motion, the velocity distribution, substructure tests, and the distribution of galaxies. In § 5, we discuss our results and an evolutionary model for A2634. Finally, in § 6 we summarize our results and the model for A2634. Throughout the paper we assume that $H_0 = 75$ km s^{-1} Mpc^{-1}.

2. OBSERVATIONS AND DATA REDUCTIONS

Multifiber spectroscopy was used to obtain redshift observations for hundreds of galaxies in the A2634 field in a time-efficient manner. We used the MX multifiber spectrometer (Hill & Lesser 1986, 1988) and the 2.3 meter telescope of Steward Observatory on 1988 June 13–15, September 11–15, and November 4–8. The MX uses 2″ diameter optical fibers positioned using microprocessor-controlled mechanical arms. We measured 528 suspected galaxy positions to 0″.5, first using the KPNO two-axis grant measuring engine and KPNO glass copies of the POSS, and subsequently using the digitized "quick V" survey plates from STScI. We then created "target" files which contain the positions of galaxies to be observed simultaneously in a 45′ field. The cD and the other bright galaxies were prioritized highest for observation. There are typically 30 object fibers and 27 sky fibers for each 50–60 minute exposure. The fibers channel the object (a galaxy) and sky light into the f/9 Cassegrain spectrograph. A 300 groove mm^{-1} grating is used to produce spectra in the 3800–6700 Å spectral range with 11 Å resolution. The detector was a UV flooded TI 800 × 800 CCD chip.

2.1. *Data Reduction Procedure*

All reductions of our data were performed using the IRAF[1] reduction package. The CCD data base included comparison lamp spectra, galaxy, and sky spectra (hereafter "objects"), bias frames, dark frames, and specialized flats. The object spectra, HeNeAr comparison spectra, and "fiber" flats are all in multifiber format and are taken consecutively to minimize fiber position distortions due to flexure. Since we were simply after radial velocities, we streamlined our reduction procedure. We performed an overscan and bias subtraction on all CCD frames, however we did not perform a flat-field correction. (We compared the final velocities obtained including a flat-field reduction to those without; the differences in velocities were very small, 14.5 and 6 km s^{-1}, for the rms and mean difference, respectively.)

The multifiber reduction began with finding the positions of the spectra on the CCD frames. Appropriately sized apertures were defined to contain each spectrum. A function for the positions of these apertures across the middle of the fiber flat was fit. This solution for the aperture position was applied to the comparison lamp and object frames. The light within each aperture was summed into a 1 pixel wide spectrum. A solution for wavelength as a function of pixel position was fit using the comparison and applied to the object frame. Finally, individual sky lines and cosmic rays were removed.

We then inspected these spectra to pick those with signal above the sky background. Typically, about 20 galaxy apertures per exposure would contain spectra meeting this criterion. These apertures were selected for cross-correlation, which is preceded by a rebinning into a logarithmic wavelength scale.

2.2. *Cross-Correlation*

We used the IRAF task "rvxcor," later "fxcor," to perform all of our cross-correlations and to compute heliocentric velocities. These tasks are based on the cross-correlation algorithm described in Tonry & Davis (1979). The spectra were Fourier filtered with a ramp filter to remove low-frequency "waves" and high-frequency noise from the cross-correlation function (hereafter CCF).

[1] IRAF is distributed by the National Optical Astronomy Observatories, which is operated by the Association of Universities for Research in Astronomy, Inc. (AURA), under cooperative agreement with the National Science Foundation.

In our first run of all spectra, we used a single spectrum of M32 for the template (Keel 1983). Both the object and template were rebinned to the same log wavelength scale. The sampled spectral range of both object and template was 3900–6300 Å. This was the largest range in common with all of the data and it excludes the edge regions on most spectra where the pixel versus wavelength solution is less reliable. The template's velocity zero-point was recalculated by cross-correlating it with five other templates, three stellar spectra and about 50 high signal-to-noise galaxy spectra from our A2634 MX data. A correction of 41 km s^{-1} was made to all of our velocities.

We next cross-correlated six templates with 240 of our *low* signal-to-noise spectra. The six templates included the previously used M32, three other M32 spectra taken with the MX spectrometer, and two spectra of NGC 3379. We experimented with two spectral subranges: 3900–4500 and 5000–6300 Å. We found that the full range (3900–6300 Å) was best for the purpose of judging the reliability of peaks in the CCF. We also found that, for low signal-to-noise spectra, even agreement between templates does not assure that the velocity is correct; a high cross-correlation peak and agreement between redundant observations of the galaxy are the best assurance of an accurate velocity.

2.3. *Errors*

We distinguish between two uncertainties in the cross-correlation process. One is the uncertainty in the position (e.g., centroid) of a CCF peak, and the other is the uncertainty that the chosen peak is the correct one (rather than one caused by chance alignment of noise and features in the object and template). The former is ≈ 100 km s^{-1}, while the latter could be over 10,000 km s^{-1}.

Both of these uncertainties were evaluated using the ratio

$$\mathrm{TDR} = \frac{h}{\sqrt{2}\sigma}, \qquad (1)$$

(called "r" in Tonry & Davis 1979), where h is the CCF peak height (mentioned above), and σ is approximately the rms fluctuations in the CCF (actually calculated from the antisymmetric component of the CCF). First, we found that CCF peaks with TDR > 3.5 were likely to be correct ones. (We determined this by inspecting redundant observations of a galaxy.) This cutoff depends on the spectral range used and should not be used with all data. We developed the categories 1 and 2 (hereafter C1 and C2) to separate velocities which were determined from CCF peaks having TDR $\geq$ 3.5, and TDR < 3.5, respectively. Second, we again used galaxies with multiple observations to plot velocity deviation versus TDR for 130 spectra; we fit a curve to this plot in Figure 1. Each point is an average of ≈ 10 measured velocity deviations. Each deviation is the difference between a given spectrum's velocity and the "best guess" velocity for that galaxy. The "best guess" velocity, in turn, was usually an average of all velocities found for that galaxy. The result is very similar to that found by Tonry & Davis (1979). For convenience, we fit our curve with a second degree polynomial. We used this curve to get a reasonable estimate for the errors of all C1 velocities by finding the highest TDR among a galaxy's spectra and locating the corresponding error on the fitted curve.

Our C1 errors are given in column (6) of Table 1. Several other comments about the errors are in order. First, there are no errors given for C2 velocities. If the correct peak was chosen for the C2's, their errors should be at least 200 km s^{-1}. Second, in the cases of three or more spectra with a TDR > 3.5, we used a standard deviation of the velocities for the error. This is because several independent measurements of the same quantity have an error best represented by a standard deviation. This would be the best approach for all galaxies if there were enough observations. Third, some galaxies were promoted from C2 to C1 during the second reduction of low-signal spectra, and a different algorithm was used for these errors. Since they were low-signal cases, we decided to make their *minimum* error 150 km s^{-1}—just larger than the greatest error for C1 velocities. Some of the C1 velocities were taken from the literature; these numbers are preceded by the capitol letter L, S, B, or Z (used the same way as in the "notes" column). We assigned the error of 25 km s^{-1} to all of the Lucey et al. velocities, and 150 km s^{-1} to the Scott et al. velocities. The other sources provided individual errors for the galaxies.

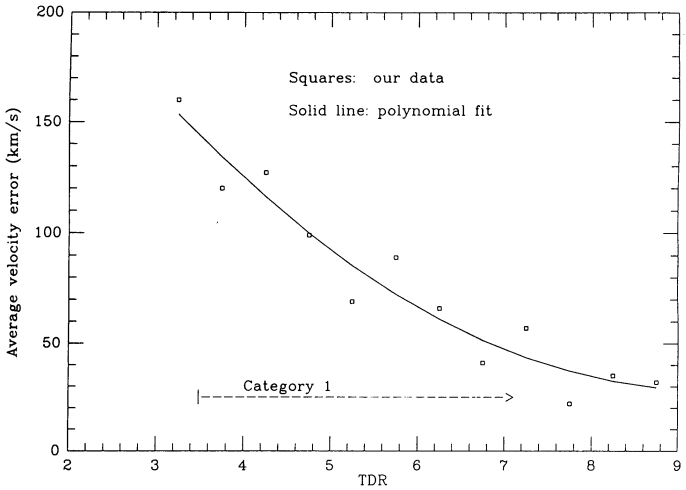

FIG. 1.—Velocity deviations as a function of correlation strength. The boxes show the average deviations of our data as a function of TDR, the "signal-to-noise" of the cross-correlation function peak. The curve is the fit used to assign errors to velocities.

An important verification of our estimated uncertainties is comparison with other published results. We were able to identify 28 of our galaxy velocities with velocities in four references. Table 2 shows all of the results of comparison with these references. The mean differences are consistent with no systematic error in our data while the standard deviations are close to our individual velocity errors, except in the case of Scott et al. (1977). Our method seems to provide velocities in good agreement with previous measurements.

3. DATA PRESENTATION

The velocities obtained through multifiber spectroscopy of the field of A2634 are presented in Table (1). The table is in order of increasing galaxy identification number, which is in column (1). Columns (2) and (3) are equinox J2000.0 right ascension and declination. Column (4) contains the C1 heliocentric velocities, and column (5) contains the C2 heliocentric velocities. Column (6) contains the velocity error based on the TDR of the CCF peak (see § 2.3 above). All velocities and their errors are in km s^{-1}. The final "notes" column contains A2634 velocities from the literature. A single letter preceding the velocity (also in km s^{-1}) signifies the publication: L for Lucey

TABLE 1

VELOCITIES AND POSITIONS OF A2634 GALAXIES

Galaxy Identification (1)	R.A.(2000) (2)	Decl.(2000) (3)	$cz(1)$ (km s^{-1}) (4)	$cz(2)$ (km s^{-1}) (5)	ϵ (km s^{-1}) (6)	Notes (7)
201	23^{h}38^{m}29^s.44	27°01′51″.6	9154.		59	cD, N7720 S9045, L9130 B9101, Z9141
202	23 38 29.58	27 02 03.6	8235.		32	"N7720A" S7911, B8229 L8088, Z8049
203	23 38 42.50	26 46 25.7	10039.		45	Z9862, S9726
204	23 36 40.75	26 41 29.2		9203.		
205	23 39 46.07	26 41 19.6		7945.		
206	23 39 09.82	26 41 35.8		8527.		
207	23 38 16.26	26 42 20.7	36792.		135	
210	23 37 25.96	26 42 45.2	25752.		126	
211	23 38 37.05	26 43 16.6		5609.		
213	23 37 27.35	26 45 02.7		8934.		
214	23 38 06.72	26 44 55.7		10400.		
215	23 39 20.61	26 45 10.1	9424.		30	
218	23 38 04.95	26 46 09.7		8812.		
219	23 37 19.50	26 46 31.2		8891.		
221	23 38 49.85	26 47 47.4	8029.		45	
222	23 37 59.65	26 48 10.4		9409.		
223	23 37 35.12	26 48 54.3		35170.		
224	23 37 38.00	26 49 08.3		9598.		
225	23 37 00.40	26 49 15.7		31141.		
226	23 38 16.08	26 49 01.9	8752.		45	
228	23 38 28.61	26 49 06.5	9526.		39	S9509, Z9542
229	23 37 31.59	26 50 13.4	8381.		44	
230	23 38 55.26	26 50 36.8	38628.		142	
231	23 39 10.37	26 50 42.4	9381.		121	
233	23 38 44.18	26 51 02.6	9105.		45	
234	23 38 55.58	26 51 19.5		10282.		
236	23 39 33.66	26 52 14.8		8802.		
237	23 37 20.11	26 52 40.8	8626.		50	
238	23 38 18.48	26 53 12.7	L9348		25	S9244
239	23 39 07.05	26 53 16.0	8762.		100	
241	23 39 34.41	26 53 39.2		12522.		
242	23 37 13.23	26 54 18.8	9650.		122	
243	23 38 09.47	26 55 13.3	9801.		105	
244	23 38 17.19	26 55 41.3	8888.		70	
246	23 38 52.48	26 56 21.8	8965.		91	
248	23 38 56.39	26 56 54.6		9372.		
250	23 39 01.49	26 57 31.1	9056.		60	L9043
251	23 37 09.47	26 58 01.5		8692.		
253	23 38 14.29	26 58 02.3	9310.		122	L9446
255	23 37 46.65	26 58 50.6	L11106		25	
256	23 38 34.47	26 58 46.0	Z8515		31	S9694, L8556
257	23 38 29.21	26 58 43.1	9546.		103	Z9600, L9538, B9605
259	23 38 26.85	26 59 06.1	10820.		48	B10819, Z10880 L10873, S10859
261	23 39 06.85	27 00 36.0	8898.		76	
263	23 38 38.81	27 00 40.4	Z9296		28	S9218, L9293
264	23 38 50.66	27 00 56.7	9970.		61	L10023
266	23 37 33.62	27 01 35.4	41327.		76	
267	23 38 10.22	27 01 49.4	8378.		73	L8398
271	23 38 36.28	27 01 46.5	Z8378		34	L8491
272	23 38 53.00	27 02 00.1	B9940		50	
273	23 38 18.62	27 02 06.8	L9552		25	
275	23 38 33.26	27 02 05.2	L9828		25	
276	23 39 30.67	27 01 55.2	8828.		73	
277	23 38 43.10	27 02 30.8	L9195		25	
280	23 38 20.68	27 03 02.8	10111.		34	L10201, B10204
282	23 37 01.98	27 03 40.7	10378		150	
283	23 38 42.65	27 03 26.3	B9983		50	
284	23 37 27.03	27 03 59.2		9353.		
285	23 39 27.41	27 03 47.5	9710.		183	
286	23 37 56.09	27 04 10.7	18429.		74	
287	23 37 26.01	27 04 17.3	10072.		54	Z10075
288	23 38 39.05	27 04 14.9	B9580		50	
293	23 38 03.04	27 05 21.4		25798.		
294	23 37 53.68	27 05 18.4	L9898.		25	
295	23 38 27.13	27 05 25.3	L7532.		25	B7684
296	23 37 55.38	27 06 01.7	10187.		71	L10160
298	23 39 02.69	27 06 08.9	10144.		88	
301	23 38 42.07	27 07 06.8	9607.		47	L9554
302	23 39 11.91	27 06 55.0	7552.		76	S7499
303	23 38 49.26	27 07 22.2	9066.		50	L8990
305	23 37 19.96	27 08 50.0	9185.		57	
306	23 39 37.74	27 08 49.5		9729		
308	23 38 22.75	27 09 28.9	9302.		22	Z9280, L9332
311	23 39 11.90	27 09 35.7	7919.		114	
312	23 38 56.24	27 09 41.4	9276.		32	L9217
315	23 39 33.69	27 09 56.6	9375.		62	
316	23 38 46.26	27 10 20.1	9944.		36	
317	23 37 55.62	27 11 12.8	37679.		146	
318	23 38 02.20	27 12 08.4	37540.		131	
319	23 38 29.14	27 12 24.7	8403.		144	
320	23 39 07.03	27 12 20.7	9751.		95	
321	23 38 41.72	27 12 54.1	8548.		141	
322	23 38 50.11	27 12 53.5	9139.		56	S9201
323	23 39 01.42	27 12 58.5	9032.		150	
324	23 38 43.66	27 12 54.9	9279.		39	S9458, Z9415
326	23 39 01.81	27 13 24.3	10488.		38	
327	23 39 19.02	27 14 44.1	9639.		32	S9695
329	23 38 58.77	27 15 18.5	8666.		72	
330	23 37 57.81	27 15 51.5	10204.		77	
331	23 38 50.66	27 16 03.9	9297.		39	Z9345, S9240
334	23 39 28.43	27 17 49.2	9310.		36	
335	23 36 56.48	27 18 22.2		9620.		
336	23 39 01.51	27 17 59.9	9832.		85	
337	23 38 20.93	27 18 14.0	9980.		116	
339	23 39 09.26	27 18 25.9	7577.		150	
342	23 39 33.94	27 19 51.3	10138.		88	
343	23 38 36.02	27 21 00.2	36975.		126	
365	23 42 01.43	26 24 58.2	9481.		143	
367	23 40 44.60	26 27 06.3		8022		
368	23 40 32.09	26 29 32.3	9690.		30	
370	23 40 46.02	26 33 18.4	9245.		150	
371	23 39 53.61	26 33 37.1	22358.		144	
373	23 40 41.24	26 36 40.5	8365.		106	

TABLE 1—*Continued*

Galaxy Identification (1)	R.A.(2000) (2)	Decl.(2000) (3)	$cz(1)$ (km s^{-1}) (4)	$cz(2)$ (km s^{-1}) (5)	ϵ (km s^{-1}) (6)	Notes (7)
374	23 41 15.75	26 36 39.7	53132.		105	
375	23 40 57.42	26 37 53.8		18976.		
376	23 40 29.28	26 38 17.3		8872		
384	23 37 45.90	26 01 23.8		31228		
389	23 38 58.06	26 03 41.1	18340.		93	
393	23 39 18.86	26 05 29.6		12686		
394	23 38 37.57	26 05 44.4		18792		
401	23 36 49.32	26 08 24.6		31133		
406	23 38 46.98	26 10 50.9	8699.		34	
408	23 38 56.49	26 12 05.2		11662.		
409	23 38 50.03	26 12 07.6	9086.		31	
411	23 39 11.55	26 13 31.7		26639.		
412	23 39 13.14	26 14 40.3	26395.		134	
413	23 37 13.53	26 16 27.5	28945.		55	
416	23 39 05.90	26 17 32.5		11879.		
421	23 36 58.45	26 21 30.2	18237.		88	
422	23 39 14.24	26 21 33.2	11690.		30	
425	23 39 35.85	26 23 35.0	18403.		111	
427	23 39 19.10	26 25 41.5		9159.		
428	23 37 45.72	26 26 50.9	9598.		88	
429	23 39 23.83	26 27 14.2		35017.		
430	23 38 00.15	26 27 33.9	9099.		61	Z9104
431	23 39 38.08	26 28 06.1		11884.		
432	23 39 15.49	26 28 14.5		27210.		
433	23 38 12.54	26 29 39.3	9206.		37	
436	23 37 45.01	26 30 17.7	8648.		63	Z8682
437	23 36 52.43	26 30 35.8	9612.		30	
439	23 39 28.24	26 32 23.8	38951.		109	
440	23 38 06.73	26 33 24.1		9637.		
441	23 38 34.32	26 33 25.6	9360.		72	
442	23 39 30.19	26 33 34.7		19248.		
443	23 39 01.68	26 33 56.5	10542.		39	
446	23 38 00.86	26 34 48.7	25915.		96	
447	23 38 48.70	26 35 50.0		12314.		
450	23 39 15.23	26 37 21.9		9717.		
451	23 37 27.74	26 37 57.5	9790.		77	
452	23 36 46.32	26 39 45.8		6759.		
477	23 36 04.33	26 32 10.0		9866.		
482	23 36 26.75	26 39 19.7		12205.		
485	23 39 55.11	26 40 27.4	8686.		64	
486	23 40 59.89	26 40 16.9	9484.		70	
487	23 42 09.32	26 40 17.2		6038.		
488	23 41 34.16	26 40 35.5		28002.		
489	23 42 30.72	26 40 40.1		17223.		
490	23 41 16.80	26 42 05.5		10981.		
491	23 41 32.37	26 42 09.2		28595.		
492	23 41 31.87	26 42 42.3		11393.		
498	23 40 37.22	26 47 29.9	11488.		32	
499	23 41 15.49	26 48 04.0	11423.		33	
502	23 41 59.50	26 48 37.5	28422.		129	
503	23 40 50.53	26 49 51.0	8838.		67	
504	23 39 58.59	26 50 02.8	8659.		20	S8657
506	23 40 46.81	26 50 06.8	11797.		42	S11560
508	23 42 42.65	26 50 29.9	17025.		111	
509	23 40 33.23	26 51 21.2	11548.		150	
512	23 40 33.12	26 53 04.1		11755.		
515	23 41 09.14	26 54 03.2		8770.		
516	23 40 12.00	26 54 22.7		19322.		
517	23 42 47.23	26 53 47.4	17213.		124	
518	23 41 26.21	26 54 23.1	23148.		69	
519	23 42 13.57	26 55 53.8	8501.		114	
522	23 42 38.13	26 58 15.9	28734.		134	
527	23 42 46.30	27 03 10.1	7536.		83	
528	23 42 38.34	27 05 29.3	7658.		63	
529	23 40 28.23	27 06 31.1	11573.		112	
530	23 41 52.56	27 07 15.1	7823.		127	
531	23 40 43.17	27 07 45.8		9391.		
532	23 40 04.22	27 08 01.8	9985.		68	
534	23 40 00.83	27 08 00.0	9455.		75	S9534
535	23 42 40.95	27 07 30.0		7673.		
536	23 42 40.51	27 08 18.0		28615.		
537	23 41 53.14	27 08 44.3		41797.		
538	23 40 03.22	27 10 00.6		8968.		
539	23 41 32.88	27 10 04.4	12450.		150	
540	23 40 42.50	27 10 39.5	10587.		144	
543	23 40 22.17	27 11 03.7	10047.		73	
544	23 40 05.33	27 11 18.7	9564.		68	
545	23 41 20.82	27 12 28.1		9068.		
546	23 40 52.79	27 12 43.2	10667.		141	
548	23 40 33.59	27 14 31.5	10901.		41	
549	23 40 52.68	27 14 57.1	8987.		35	
550	23 40 52.12	27 16 23.7		11948.		
555	23 40 35.71	27 18 41.8	23236.		39	
557	23 40 12.51	27 20 03.6	20884.		92	
561	23 34 38.72	26 43 24.4	Z9700.		28	
570	23 36 17.49	26 50 19.8	8637.		65	
572	23 34 22.68	26 53 02.5	20489.		80	
573	23 34 13.07	26 54 42.7		38254.		
574	23 36 38.90	26 54 34.2	8934.		123	
575	23 36 01.59	26 55 04.4		31058.		
576	23 35 44.03	26 56 10.8		36901.		
578	23 36 14.44	26 59 24.1		36481.		
579	23 35 49.93	26 59 43.4	7316.		135	
580	23 35 06.33	27 01 20.7	16906.		77	
581	23 35 14.86	27 02 20.2	17373.		61	
584	23 35 33.63	27 05 10.1		13122.		
586	23 34 31.50	27 07 28.5		9585.		
588	23 35 56.97	27 10 27.0	18673.		150	
589	23 35 25.15	27 11 08.6		15286.		
590	23 35 23.46	27 11 47.0		36852.		
591	23 35 29.86	27 11 46.1	18855.		150	
592	23 35 14.36	27 11 59.6	30570.		105	
597	23 34 59.51	27 13 00.1	17621.		111	
598	23 36 23.64	27 13 19.5		19667.		
599	23 33 44.79	27 13 42.5		32320.		
602	23 35 54.32	27 15 22.2	19252.		114	
604	23 36 10.13	27 16 05.7	18320.		95	
605	23 36 38.84	27 18 22.1	8415.		125	
606	23 33 40.53	27 18 59.2		9474.		
607	23 35 23.14	27 19 21.9	17750.		114	

TABLE 1—*Continued*

Galaxy Identification (1)	R.A.(2000) (2)	Decl.(2000) (3)	$cz(1)$ (km s^{-1}) (4)	$cz(2)$ (km s^{-1}) (5)	ϵ (km s^{-1}) (6)	Notes (7)
609	23 34 40.01	27 19 50.6	8893.		58	
610	23 35 19.37	27 19 57.7	19536.		49	
612	23 35 14.22	27 20 14.9	18878.		51	
615	23 35 10.50	27 21 35.2	18645.		102	
616	23 35 18.44	27 21 41.5	37018.		63	
621	23 40 33.04	27 23 02.8	10404.		75	
627	23 41 33.23	27 30 19.1		9798.		
628	23 40 54.25	27 30 33.5	10040.		45	
630	23 41 24.38	27 31 53.3	10033.		43	
631	23 40 46.81	27 32 18.9	10307.		61	
633	23 41 34.70	27 33 23.5	17594.		150	
635	23 40 19.08	27 33 41.0	8696.		60	Z8707
642	23 40 45.52	27 40 13.2	9565.		94	
658	23 39 25.58	27 22 34.6	17120.		140	
659	23 39 49.36	27 22 33.4	10081.		41	
661	23 39 08.66	27 24 22.2		8696.		
662	23 38 13.66	27 24 50.4	9285.		56	
664	23 39 34.58	27 27 05.0	37981.		109	
670	23 36 53.38	27 33 06.7		13850.		
671	23 39 13.42	27 32 54.0	9222.		72	
680	23 39 22.60	27 34 47.1		37816.		
681	23 39 33.22	27 35 31.2	37114.		144	
693	23 34 44.04	27 23 15.4	18739.		33	
699	23 36 26.00	27 23 53.5	9133.		31	
700	23 34 45.61	27 25 30.4	18158.		76	
703	23 34 41.68	27 29 56.7	18211.		66	
704	23 35 57.17	27 32 02.6	18236.		39	
705	23 34 42.52	27 32 57.6	16962.		30	
707	23 34 41.18	27 37 30.8	18775.		141	
709	23 35 48.22	27 38 36.0	18402.		82	
710	23 36 14.34	27 38 43.9	20165.		150	
1381	23 37 24.10	27 14 32.8		37923		
1310	23 38 32.17	26 54 34.6	8270.		98	
SRT2	23 41 18.78	27 09 38.5	9271.		150	
Z13	23 38 38.38	27 00 37.4	9356.		38	
Z18	23 39 30.53	27 00 37.7	10837.		28	
L1261	23 38 53.93	27 02 45.6	9643.		25	

et al. (1991), S for Scott et al. (1977), B for Bothun & Schombert (1988), and Z for Zabludoff, Huchra, & Geller (1990).

Of the 528 objects identified in the 2° × 2° field of A2634, more than one-half were observed with the MX. Many of these galaxies had counts too low above the sky level to warrant cross-correlation. 108 C1 and 46 C2 velocities were obtained of A2634. Eighteen velocities for A2634 were added from the literature and are considered C1. No foreground galaxies appeared, except a few low-velocity galaxies in A2634 which may be members of A2666 to the east (see below). Many background galaxies were discovered in the field; 29 C1 and 6 C2 galaxies were clustered around 18,000 km s^{-1}. A smaller subset of galaxies belong to a cluster near 40,000 km s^{-1}. The positions of the objects in the field are shown in Figures 2*a*–2*c*.

TABLE 2

COMPARISON OF OUR A2634 VELOCITIES WITH THOSE OF OTHER REFERENCES[a]

Reference	Number	Mean Difference (km s^{-1})	Standard Deviation (km s^{-1})
Lucey et al.	14	1.8	72.7
Scott et al.	13	53.6	176.3
Bothun & Schombert	5	−18.4	80.9
Zabludoff et al.	13	2.4	89.2

[a] See § 2.3.

A histogram of all C1 velocities is shown in Figure 3. Large-scale structure is revealed in the clumpy distribution of galaxies in redshift space. There are three noticeable concentrations: A2634 is the nearest cluster at 9000 km s^{-1}, followed by a concentration at 18,000 km s^{-1} and a sparser concentration at 40,000 km s^{-1}. We used the midpoint between the first two concentrations to define the A2634 upper boundary. Also, we have no velocities below 6000 km s^{-1}. Hence, our initial membership criterion for A2634 is velocity between 6000 and 14,000 km s^{-1}.

Figure 4 depicts the radio, optical and X-ray data for the cluster field. A2634 galaxies with C1 velocities are represented by crosses. The X-ray contours come from the *Einstein* X-ray Observatory IPC map (see Eilek et al. 1984), and the 6 cm radio map is from the VLA. The radio source is the wide angle tail prototype, 3C 465. Its core coincides with the cD nucleus and is located at the peak of X-ray emission (the X-ray position is known to within $\approx 1'$). There is a previously unidentified X-ray clump to the northwest of A2634. A new CCD frame (F. Owen 1992, private communication) reveals a distant cluster of galaxies coincident with this X-ray clump. Some of our measured 37,000 km s^{-1} galaxies (Fig. 4) are apparent members of this background cluster.

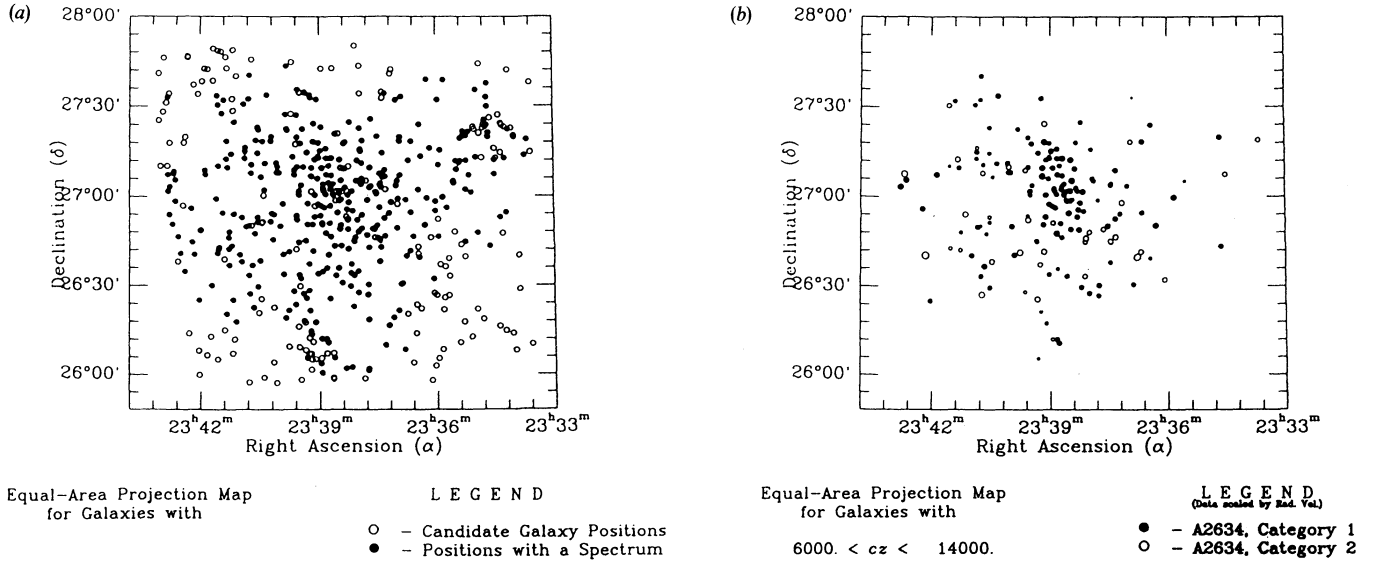

FIG. 2.—Plots of galaxy positions in the A2634 field. Fig. 2*a* shows the fairness of our sample by plotting objects for which we obtained a spectrum as filled circles on top of all 528 objects for which we measured a position. Fig. 2*b* separates the A2634 galaxies from the foreground and background objects using the velocity criterion $6000 < V_{member} < 14{,}000$ km s^{-1}. C1 and C2 are defined in § 2.3. Fig. 2*c* shows the positions of background galaxies. The galaxies clustered to the northwest have $V \approx 18{,}000$ km s^{-1}. For both Figs. 2*b* and 2*c*, the smaller the circle, the larger the redshift.

4. ANALYSIS

In this section we present the analysis performed on our A2634 data given in Table 1. We will start by attempting to quantify the fairness of our velocity sample. We will then look at the centroid, ellipticity, and position angle of the spatial galaxy distribution. Next, we describe the statistical estimators used to find the velocity centroid and dispersion and give those results. The cD peculiar motion is then calculated. Finally, we discuss the normality of the distribution followed by an investigation of substructure.

We have used the C2 sample in our substructure analysis but omitted them from other calculations. The C2 velocities are accurate enough to say that they are associated with galaxies in or near the cluster's redshift, and their sky positions are as certain as the C1s so that they are useful for substructure information. However, the C2 velocities and their errors are not well-determined and thus should not be allowed to affect velocity centroid, dispersion, normality, and peculiar motion calculations.

4.1. *Fairness of Sample*

A goal of this project is to accurately measure the cluster's location and scale (traditionally, mean and standard deviation) in velocity space. When estimating these quantities there is an implicit assumption that the measured velocity distribution is a fair sample of the true velocity distribution. This, in turn, depends on how fairly the spatial galaxy distribution is sampled because dynamical properties depend on position in the cluster. (For example, the velocity dispersion should decrease at large radii for a relaxed cluster.)

We compared numbers of galaxies in annuli centered on the cD, and in four quadrants with a common vertex at the cD. We

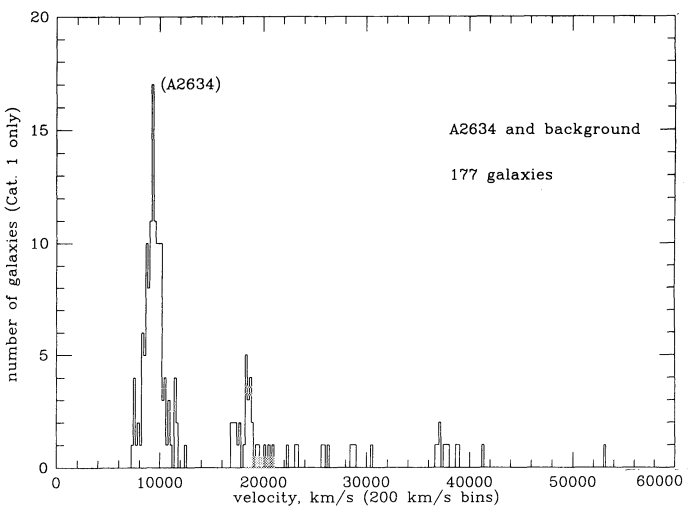

FIG. 3.—Histogram of all C1 velocities in the A2634 field

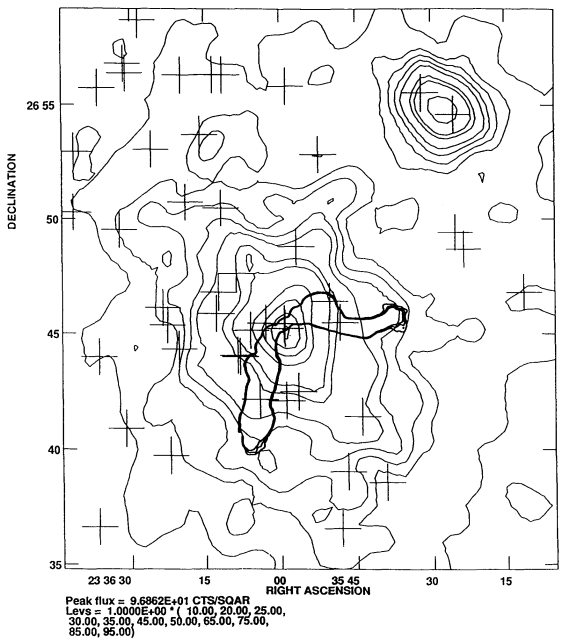

FIG. 4.—A2634 in radio, optical, and X-ray. The contours are of an *Einstein* IPC X-ray image (Eilek et al. 1984), 3C 465 is outlined with a bold contour from a 6 cm VLA map, and the crosses represent galaxies in A2634 and background (the two in the northwest X-ray blob) for which we have measured velocities.

took our 528 measured positions in the field to be our "parent population." Our comparison subsample consisted of 355 positions of all objects for which we obtained a spectrum. Figure 2*a* qualitatively shows the fairness of this sample (*filled circles*). The ratios of galaxy counts reflect some of the obviously undersampled regions, like the lower right quadrant. The ratios of quadrant counts from the two samples show an $\approx 7\%$ maximum variation. A chi-squared test indicates that there is a 99.1% probability that the two distributions are the same. The annular count ratios in 12 concentric, 5′ wide annuli show a larger variation. They indicate roughly constant sampling ratios of 80 to 90% between the first and eighth annuli, but the last four ratios drop from 0.74 to 0.48, indicating an undersampling between 45′ and 60′. A chi-squared test of the annular counts shows that there is a 62% chance that the two distributions are the same.

Some of the reasons for this unfairness in annular sampling are related to our observing priorities. The inner regions are more profitable hunting grounds for cluster members; the inner MX fields were probably reobserved at the expense of outer fields. The innermost annulus was also highly sampled because of the addition of velocities from papers which preferentially sampled this region (especially Bothun & Schombert 1988). The chi-squared results imply that we evenly sampled the field azimuthally, but the annular count ratios show some unevenness with radial distance. If this were a relaxed cluster, the effect of undersampling outer regions would be to slightly increase the measured velocity dispersion. We emphasize that for nine consecutive annuli the count ratios remained fairly constant and these encompass 79% of the sampled objects. We assess the effect of the gradient in annular counts as not being serious for our location and scale estimates, but worth noting.

4.2. *Asymmetry in the Cluster*

In the previous section, we inspected the spatial distribution of 355 objects with spectra. If we now use a membership definition of 6000–14,000 km s^{-1} to remove all but 126 C1 velocities, we can investigate the symmetry of A2634. This sample may be the best for representing the cluster's spatial distribution. The sampling unevenness that we found in the $N = 355$ sample (previous section) should be repeated here if the $N = 126$ sample is *symmetrically distributed* about the cD, i.e., it should have a roughly constant ratio to the parent population's ($N = 528$) distribution for the four quadrants, and a slightly decreasing ratio to the parent population with radius. If we count galaxies in four quadrants as done in the previous section, we find that the cluster galaxies prefer the east side more than was found for the $N = 355$ subsample. A chi-squared comparison of the cluster's quadrant counts with those of the parent population gives only a 3% probability that the two distributions are the same, whereas the $N = 355$ sample had an 83% probability. Similarly, the chi-squared comparison of the annular counts goes from 54% for $N = 355$, to 0.2% for $N = 126$. This is due to a greater tendency for the member galaxies to bunch near the center (which we define by the cD) than the background galaxies and stars that are included in the $N = 355$ sample (see Fig. 2*c*). Moreover, a direct chi-square comparison of the $N = 355$ sample to the $N = 126$ sample gives a 3.9% and 6.5% probability of agreement between the quadrant and annular counts, respectively. Because the chi-squared test takes into account Poisson noise, the $N = 126$ sample shows significantly more asymmetry than the $N = 355$ sample.

We also used more rigorous techniques to describe this sample's spatial distribution. The Fourier and tensor methods of determining ellipticity and position angle are described in Rhee, van Haarlem, & Katgert (1991). A simple mean of galaxy positions gives the cluster centroid. We found that the centroid of the 126 galaxy sample was 7.5 east and 1.1 south of the cD. The ellipticity of the cluster was found to be 0.26 using the tensor method and the cD as the cluster center. The position angle of maximum elongation was $55° \pm 12°$ using the Fourier method. The ellipticity is about equal to the average found for a sample of 107 rich clusters (Rhee et al. 1991).

4.3. *Location and Scale*

We next determined the location (e.g., velocity mean), scale (e.g., velocity dispersion), and corresponding confidence intervals of our sample. We used the estimators calculated by the program "ROSTAT," provided by Beers, Flynn, & Gebhardt (1990, hereafter BFG). Recommendations are given for which estimators to use with a given sample size based on numerous simulations. For large sample sizes such as ours, BFG recommend the biweight for an estimator of location and scale. These are represented by $C_{\rm BI}$ and $S_{\rm BI}$, respectively. These estimators are resistant to outliers and are robust; they do not require assumption of an underlying distribution (e.g., Gaussian). The definitions for these and other estimators are found in BFG as well as Teague et al. (1990). The error for the biweight estimate of location is analogous to the error in the mean for a normal distribution, $\sigma/\sqrt{N}$, except that the biweight estimate of scale is used in place of σ: $S_{\rm BI}/\sqrt{N}$. The confidence interval recommended for our scale is called the "jackknifed" biweight interval, defined in BFG. We show only the values of these errors corresponding to the 68% significance level.

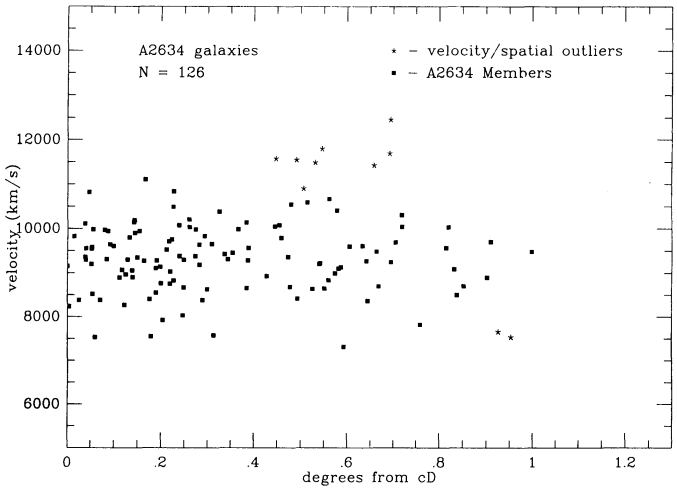

FIG. 5.—Radial velocity vs. distance from the cD galaxy. The $N = 126$ analysis sample is represented by filled squares except for the 10 extreme velocity/spatial outliers (discussed first in § 5.1) which are represented by stars.

We have used the above statistical estimators on an A2634 sample of size 126. This sample includes the 108 C1 velocities that we have measured between 6000 and 14,000 km s^{-1}, and 18 velocities obtained from the literature. The biweight estimate of central location, with its heliocentric correction and its confidence interval is 9380 ± 79 km s^{-1}. The biweight estimate of scale, including relativistic and measurement error corrections (Danese, DeZotti, & di Tulla 1980), is 886 ± 74 km s^{-1}. As a comparison, the traditional mean is 9432 km s^{-1}, and the standard deviation is 917 km s^{-1} (also including relativistic and error corrections). These larger values indicate that the traditional indicators lack resistance to long tails (see § 4.5).

Figure 5 depicts how the velocity distribution varies with cluster radius (distance from the cD). A relaxed cluster is expected to show a decrease in velocity dispersion with radius. Our $N = 126$ sample shows the opposite effect; however, the velocity-spatial outliers represented with stars are likely nonmembers (see § 5.1). Their removal makes A2634 consistent with a relaxed cluster.

We also found the location and scale of the background cluster concentrated to the northwest in Figure 2*c*. These 29 C1 velocities have $C_{BI} = 18{,}248 \pm 188$ km s^{-1}, and $S_{BI} = 990 \pm 180$ km s^{-1}.

4.4. *Peculiar Motion of cD*

The velocity centroid of 9380 ± 79 km s^{-1} will now be used to determine the peculiar motion of the cD in A2634. For the cD, we use the velocity from Table 1 of 9154 ± 59 km s^{-1}. Its error did not come from the TDR calibration but from the standard deviation of the velocities from its five best spectra. The errors of the centroid and the cD velocity are summed in quadrature to give the peculiar motion of -226 ± 99 km s^{-1}. This value must be corrected by a factor of $(1 + z)$ which gives the peculiar motion in the cluster rest frame, -219 ± 98 km s^{-1}.

The magnitude of our peculiar motion is not as great as that measured for some other dominant galaxies (e.g., A2670 has 440 km s^{-1}, Sharples et al. 1988; A1795 has 365 km s^{-1}, Hill et al. 1988; A2107 has 270 km s^{-1}, Oegerle & Hill 1992). Our larger sample size has resulted in low errors and a comparatively significant measurement. Teague et al. (1990) used the following formalism for the statistical significance:

$$S_V = \frac{|C_{BI} - cz|}{(\sigma_1^2 + \sigma_2^2)^{1/2}} \quad (2)$$

where σ_1 and σ_2 are the errors in biweight and cD velocity. They consider $S_V \leq 1$ to mean that the galaxy is at the dynamical center of the cluster, and $S_V = 2$ to mean the peculiar motion is marginally significant. We have $S_V = 2.23$ which implies a motion significant at the 97% level. A more complex significance algorithm was used by Gebhardt & Beers (1991). Applying their technique, we obtain an asymmetric, 90% confidence interval on the velocity centroid using a bootstrap resampling procedure from BFG. Our bootstrap confidence interval for C_{BI} is 9380^{+127}_{-122} km s^{-1} and our cD's 90% interval is 9154 ± 94 km s^{-1}. The sum of 122 and 94 is just less than the rest-frame peculiar velocity and so Gebhardt & Beers would report the peculiar motion as significant.

At this point the reader should question the use of this sample for the peculiar motion calculation for the following reason: the sample has not been weeded of nonmembers or subclusters. Our philosophy on membership is that all of the data should be analyzed before velocity outliers are removed as nonmembers. On the other hand, a small percentage of galaxies not physically associated with the cluster (e.g., 13% in A2670, Sharples et al. 1988), yet having velocities within 3 σ of the cluster mean can throw off the location estimate. Moreover, if the cluster is found to have substructure, the velocity location and scale should only be calculated for members of the subcluster containing the cD or D galaxy. We will address these questions on the following two sections.

4.5. *Normality*

In this section we discuss to what extent our velocity distribution is consistent with a Gaussian. The purpose is partly to motivate clipping techniques and partly because normality plays an important part in understanding the cluster's dynamical state (King 1966; Yahil & Vidal 1977). A velocity histogram is shown in Figure 6 containing the 126 C1 velocities between 6000 and 14,000 km s^{-1}. The cD velocity and the velocity centroid are marked. We found that the jaggedness of this histogram is consistent with histograms of randomly generated velocities from a Gaussian distribution with the same sample

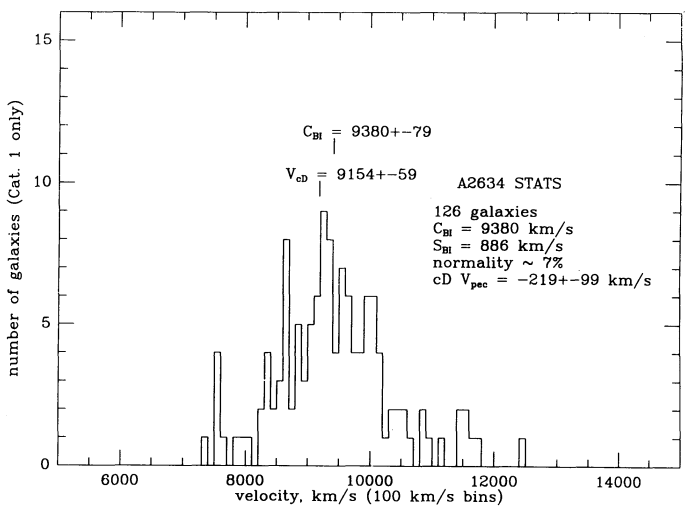

FIG. 6.—Velocity histogram of our unclipped, category 1, A2634 sample.

size and bin size. The velocities continuing out further on the right side of the centroid than the left, however, *are* inconsistent with a Gaussian distribution. We shall quantify this non-normality using 12 statistical tests drawn from ROSTAT (BFG).

The 12 test statistics used have a wide range of values for a given sample. In order to assess the meaning and significance of these numbers, their percentiles must be calibrated. D'Agostino (1986) provides definitions and percentiles for most of the tests including the B_1-test, B_2-test, B_1–B_2 Omni test, *KS*-stat, *V*-stat, W^2-stat, U^2-stat, and the A^2-stat. Martinez & Iglewicz (1981) introduce and calibrate the *I*-test. Yahil & Vidal (1977) describe the *a*, *W*, *u*, and B_2-tests. The tabulation of percentiles can be found for the *u*-test in Pearson & Stephens (1964), for the *a*-test in Pearson & Hartley (1966), and for the *W*-test in Shapiro & Wilk (1965).

Table 3 shows the values of the tests for our $N = 126$ sample, and provides the significance of our test statistics for our sample size. Most of the tests show that our $N = 126$ sample is non-normal either in kurtosis or skewness. Collectively, they tell us that we have a distribution with a long tail on the high (right) side of the mean. Most of the tests are either sensitive to skewness (asymmetry) or kurtosis (a long-tailed or sharply peaked quality); only two tests, the *B*1 & *B*2 Omni test and the *I*-test are *omni* tests, i.e., sensitive to both problems. These two both indicate that the hypothesis that our distribution is Gaussian is accepted at only the ~4% level. One may opt to use only the most powerful tests available to characterize the cluster. For kurtosis, this would be the *W*-test which finds acceptance at the 12.4% level. Only one test is sensitive to skewness alone, the *B*1-test, and this finds acceptance at only the 2.6% level; our distribution suffers more from skewness than kurtosis. The last five tests given in Table 3 are the least robust in that they compare the cumulative distribution function of the data to that of a perfect Gaussian. The *KS* statistic and the Kuiper *V*-statistic are the crudest of these five because they have poorly defined percentage points. If we average all but these two tests, we can find a reasonable assessment for the level at which the Gaussian hypothesis is accepted for our $N = 126$ distribution: 7%.

We reran the tests after clipping the highest velocity and found that the remaining distribution is accepted as Gaussian at greater than the 10% level. This was the only velocity removable under 3 σ clipping as prescribed by Yahil & Vidal (1977). The skewness and kurtosis characteristics remained but to a lesser extent. We cannot rule out that the A2634 velocity distribution is drawn from a Gaussian population because of only one galaxy which may not be a member.

TABLE 3

NORMALITY TEST RESULTS FOR OUR 126 C1 VELOCITIES BETWEEN 6000 AND 14,000 km s^{-1}.

Test Name (1)	Null Value (2)	Our $N = 126$ Value (3)	Percentile (4)	Meaning (5)
A	0.7979	0.753	1–5%	long-tail
U	≈5.2	5.4	>10	normal
W	1.000	0.972	12.4	normal
B_1	0.000	0.416	2.6	skewed
B_2	3.00	3.64	6.3	long upper tail
B_1 B_2 Omni	1.00	6.09	4.8	skewed and/or long-tail
I Omni	0.982	1.076	<5.0	skewed and/or long-tail
KS	0.000	0.760	25.0	normal
V	0.000	1.244	25.0	normal
W^2	0.051	0.116	6.8	long upper tail
U^2	0.048	0.105	7.5	long upper tail
A^2	0.341	0.790	4.1	long upper tail

NOTES.—The value of each test statistic for a perfect Gaussian are given in col. (2), marked "Null Value." The value of each test statistic for our sample is given in col. (3). Col. (4) gives the significance at which the hypothesis that the velocity distribution is Gaussian is accepted. Low percentiles imply non-Gaussian characteristics. An interpretation of each test result is provided in the fifth column.

4.6. *Substructure*

We now continue to analyze effects which can distort our peculiar motion estimate by looking for substructure in A2634. By substructure, we mean galaxies which appear close together within the cluster and also share roughly the same velocity. Such substructure could affect the apparent peculiar motion of the cD. Substructure might also suggest that the cluster is still in the process of formation rather than being relaxed (Fitchett 1988).

To quantify the substructure in our $N = 126$ distribution, we used the Dressler-Shectman (1988) δ-test. First, this test estimates the velocity mean and dispersion for the 10 nearest neighbors to each galaxy. Second, these local means and dispersions are compared with the *global* mean and dispersion (using all galaxies with velocities). A deviation from the global values can then be defined for each galaxy as:

$$\delta^2 = \left(\frac{11}{\sigma^2}\right)[(v_{\rm local} - v)^2 + (\sigma_{\rm local} - \sigma)^2] \, . \qquad (3)$$

Finally, a cumulative deviation, Δ, is defined as the sum of the δ's and serves as the statistic for quantifying the substructure. The significance of Δ is assessed using a Monte-Carlo analysis: the velocities are randomly shuffled among fixed positions 1000 times and Δ is calculated for each new sample.

The plots in Figure 7 graphically demonstrate the location and severity of possible subclustering in the actual cluster (*top*) and two of the Monte-Carlo cluster simulations (*bottom*). The upper left plot simply represents each A2634 galaxy by a filled circle. The upper right plot represents each A2634 galaxy by a circle with radius proportional to e^{δ}. Many large circles concentrated in a small area implies a deviation of local dynamical properties from the global ones. The lower left graph shows the Monte-Carlo simulation with the maximum value of Δ and the lower right graph has the median value of Δ for 100 simulations. The Δ for our cluster was 180 and it is larger than the Δ of 98.3% of 1000 simulations. The test and figures imply that there are significant deviations in local dynamical properties on the east side of the cluster. There is a conspicuous grouping of large circles in this region while most of the galaxies closely grouped around the cD have small circles.

To investigate whether the δ-test had uncovered a subcluster, we plotted the positions of galaxies in small velocity intervals. Figure 8*a* shows that three of the eight C1 galaxies with velocities between 6000–8000 km s^{-1} are on the far east side of the field; possibly members of A2666. The galaxies with velocities between 8000–9000 km s^{-1} are distributed symmetrically around the cD. When we look at the next higher velocity intervals we see the galaxies increasingly distributed in the northeast. In particular, the 10,000–10,500 km s^{-1} galaxies appear to belong partly to the cD's cluster and partly to a grouping to the northeast. If the cluster were simply elongated, the extension should be equally represented in all intervals, but

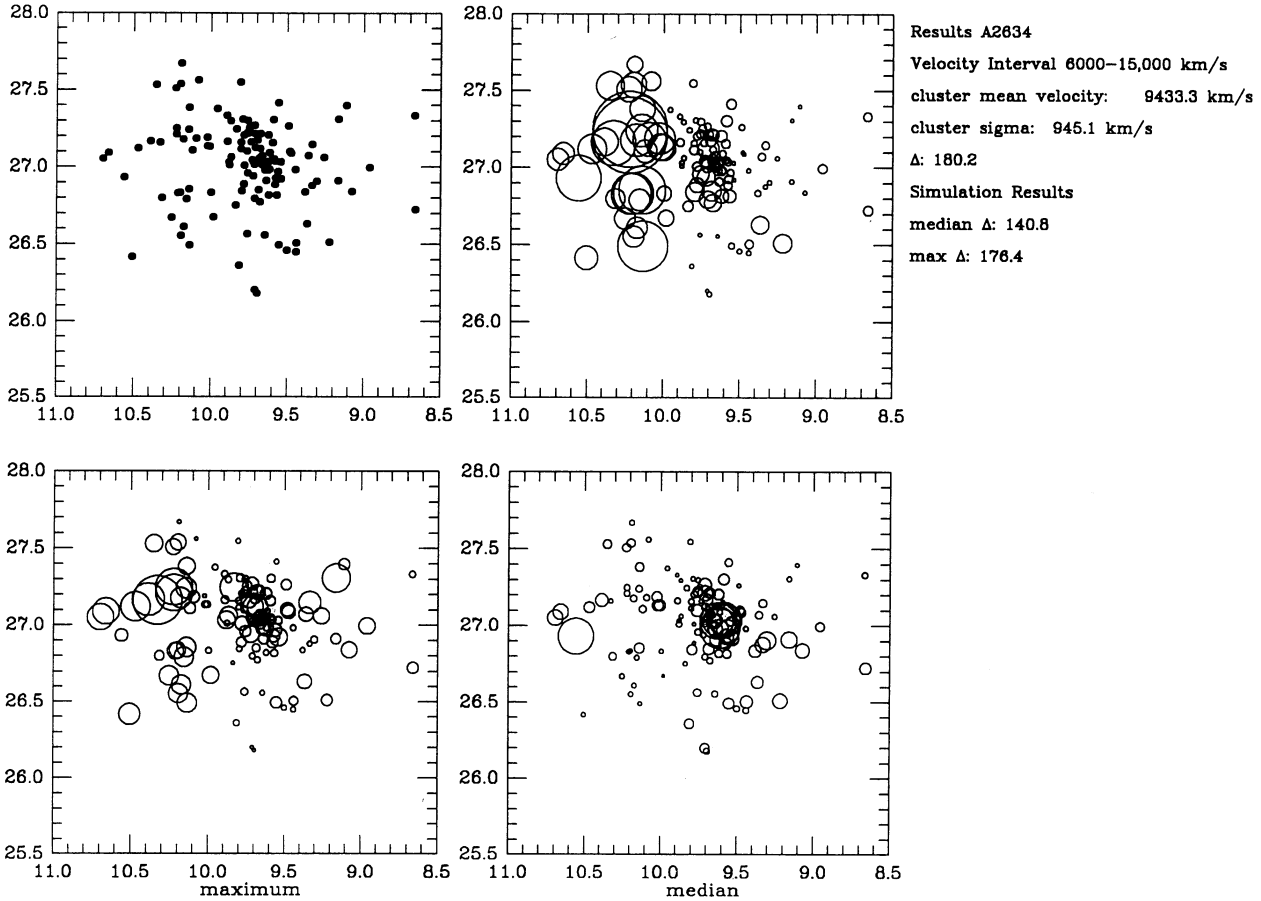

FIG. 7.—Results of the Dressler-Shectman δ-test. The upper left plot simply shows the A2634 galaxy member positions (as in Fig. 2*b*). The upper right plot represents each galaxy with a circle whose radius is proportional to the deviation of the "local" (itself and its 10 nearest neighbors) velocity mean and standard deviation from the global mean and standard deviation. The value Δ is the sum of these local deviations. The lower two plots show similar circles after the velocities have been shuffled randomly among the same positions. The maximum and median Δ-values arising from 100 random shufflings are shown.

Figure 8*b* suggests that the northeastern region has a higher mean than the central region. Figure 8*c* also shows some of the 10,500–11,000 km s^{-1} galaxies (*circles*) in the northeast region.

In the velocity interval 11,000–13,000 km s^{-1} (Fig. 8*c*, *filled squares*), the trend of clumping around the cD and the northeast abruptly ends. These galaxies are preferentially distributed on the *east* side of the cluster. Notice that four of these galaxies are clumped into a small region 12′ across. It is conceivable that this is a chance alignment, but other observations reinforce its reality. First, the C2 galaxies in this velocity bin contribute two more galaxies to the group. Second, when we analyze the six velocities we find that the group has a mean of 11,567 km s^{-1}, and a small dispersion of 171 km s^{-1}. A third C2 velocity, 10,981 km s^{-1}, is positioned in this group and may be included to make seven members with the dispersion of 271 km s^{-1}. Figure 8*c* also shows three C2 galaxies combining with a single C1 galaxy in the south of the cluster to form a second grouping. This one has a velocity mean surprisingly close to the first group, 11,780 km s^{-1}, and its dispersion is 120 km s^{-1}.

Figures 8*a*–8*c* provide explanations for the distribution of large circles in the δ-test for the $N = 126$ sample. The eastern side of the cluster is populated bv groups near 11,700 km s^{-1} and a possible subcluster to the northeast near 10,000 km s^{-1}. These have the effect of increasing the local mean above the global value. Extreme low-velocity outliers (from A2666?) and galaxies with velocities close to the mean are also mixed in to increase the local dispersion in the east above the global value. In the next section we will discuss the remaining substructure in A2634 after outlying galaxies are eliminated.

5. DISCUSSION

Our analysis has given us four primary results from our redshift data on A2634: (1) the cD has a significant peculiar velocity of -219 km s^{-1}, (2) the velocity distribution has a one-sided tail uncharacteristic of a Gaussian distribution, (3) the galaxy spatial distribution shows elongation and more galaxies on the east side of the cD than the west, and (4) the Dressler-Shectman substructure test statistic is significantly large reflecting the higher mean and dispersion on the east side of the cluster. A few small galaxy groups may occupy this region. We will now clarify these findings and discuss an evolutionary scenario for the cluster which takes into consideration the radio and X-ray data.

Throughout the previous section we analyzed a sample of 126 galaxies. The membership criteria were very lenient: the galaxies had velocities between 6000 and 14,000 km s^{-1} and the positions could be anywhere in the 2° field shown in Figure 2. This sample is likely to be contaminated with galaxies not physically associated with A2634. Thus, it would be wise to consider strategically chosen subsamples of our $N = 126$ sample and to see what our analyses give for these.

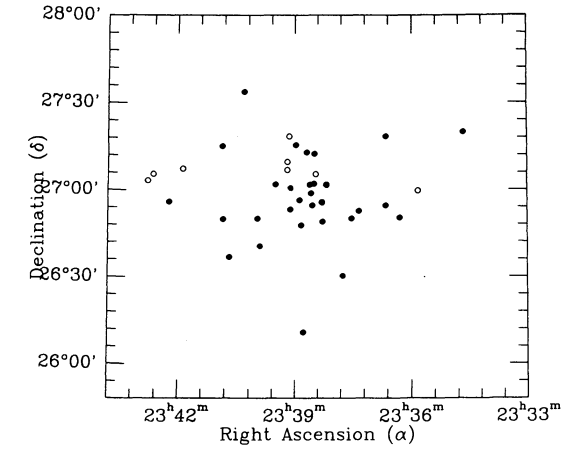

FIG. 8*a*

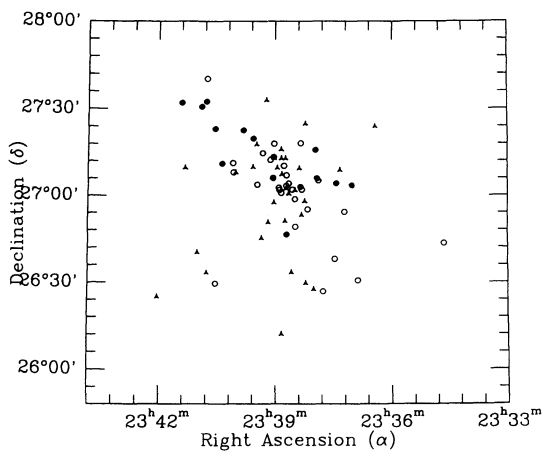

FIG. 8*b*

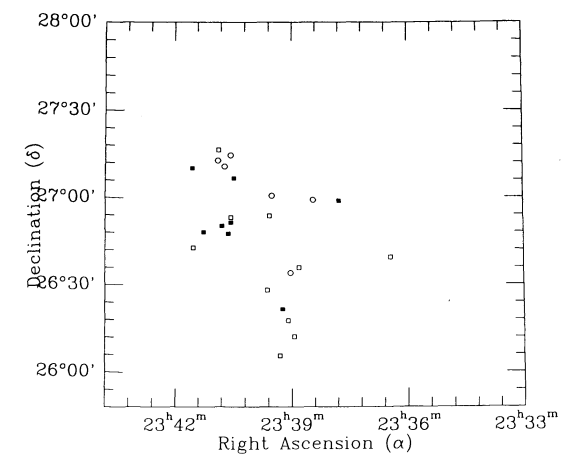

FIG. 8*c*

FIG. 8.—Positions of galaxies in seven velocity sub-intervals. Fig. 8*a* shows how the lowest velocity galaxies are in a regular arrangement concentrated around the cD position. Fig. 8*b* shows three sub-intervals which demonstrate a dependence of the northeastern elongation on velocity. Fig. 8*c* shows the distribution of the highest velocity galaxies to be primarily east of the cluster center. The spatial distribution of the C2's with $11{,}000 < V < 13{,}000$ km s^{-1} is similar to the C1's (see § 4.6).

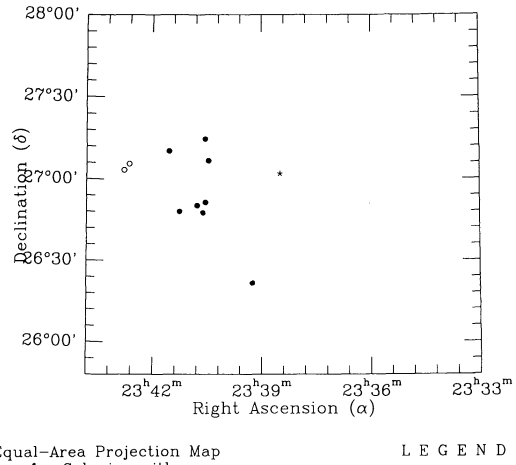

FIG. 9.—Positions of galaxies which are both spatial and velocity outliers. Clipping these from the sample leads to drastically different substructure test results (see § 5.2). The position of the cD galaxy is again shown for reference.

5.1. *Substructure Revisited*

The δ-test for substructure (Fig. 7) indicated that our $N = 126$ sample had dynamical characteristics more spatially correlated than 98.3% of the Monte-Carlo simulations. Further inspection revealed that galaxies with both high and low velocities were distributed on the east side of the cluster, some in groups, while galaxies with local dynamics similar to the cluster average are densely packed around the cD.

How is the substructure altered by removal of candidates for contamination? We found that removing only a few galaxies does not drastically reduce the overall significance as it does for the normality tests (§ 4.5); removing the two highest velocity galaxies still left Δ larger than 96% of the simulations. However, clipping of only the four galaxies in a group on the east side reduced Δ to greater than 79% of the simulations. Clipping 10 of the extreme velocity/spatial outliers depicted in Figure 9 (including the five galaxies in the two groups, two low-velocity outliers, and three more high-velocity outliers) reduced the cluster's Δ to greater than only 70% of the simulations. The remaining large circles are exclusively in the NE region of the cluster (Fig. 10).

Interpretation of these substructure results takes very different directions depending on how many of the $N = 126$ sample one keeps as members of A2634. Using the standard 3 σ clipping algorithm removed only 1 high-velocity outlier from our $N = 126$ sample, so we may not be justified in eliminating all 10 outliers from membership. In this case, the cluster must be in an unrelaxed state because of the anisotropic velocities on the east side of the cluster. The cluster might then also contain one or two subclusters on the eastern and southern edges of the field (Fig. 8*c*).

We have investigated the role played by Abell 2666 in the $N = 126$ substructure. This cluster has a velocity dispersion of

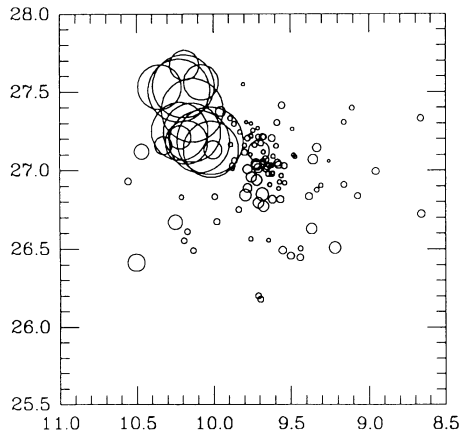

FIG. 10.—Results of the Dressler-Shectman δ-test after 10 possible contaminating galaxies are removed. Large circles are located to the northeast of cluster center reflecting the deviation in mean of those velocities. The value of Δ is only greater than that of about 70% of Monte Carlo simulations.

476 km s^{-1}, a velocity centroid of 8095 km s^{-1} (Zabludoff et al. 1990), and it is 2.'8 east of the cD in A2634. It is suspicious that the dynamical disturbances of A2634 are located so close to A2666, however, we do not find that tidal forces or infalling groups along a supercluster filament are credible scenarios. It is more likely that 2–3 of the easternmost galaxies with velocities between 7000–8000 km s^{-1} (Fig. 8*a*) are members of A2666. These contribute to the large dispersion on the east side of A2634.

Two possible interpretations are reached when one assumes that the 10 spatial/velocity outliers clipped above are not members of A2634. The level of remaining substructure by the δ-test is not significant but the arrangement of large circles (Fig. 10) suggest a region of deviant mean and standard deviation to the NE. Thus, one could interpret this to be insignificant and that the cluster is free of substructure, or the cluster contains two components; one centered on the cD and the other to the NE of the cD. Either way, the clipping also has an interesting affect on the normality and spatial distribution (to be discussed next). In § 5.5 we further discuss the interpretation that the northeast component is real.

5.2. *Spatial Distribution*

The removal of the 10 likely nonmembers discussed above also influences our calculations of the cluster centroid, ellipticity, and position angle (PA) for A2634. We found that the centroid was less distant from the cD; 5.'2 east and 0.'7 south. The ellipticity of the cluster increased to 0.28 (tensor method). The PA became 46° ± 11° using the Fourier method, again with the cD as the center. The elongation is more pronounced after removal of the outliers, as is seen in the smaller error in the position angle. The remaining offset of the centroid from the densest concentration of galaxies (near the cD) may be due to the remaining extension to the northeast (Fig. 8*b*).

The appearance of Figures 7 and 10 suggest that only the dense, inner clump of galaxies are reliable and substructure-free members of A2634. A spatial analysis of only 88 galaxies in this inner clump found a centroid much closer to the cD (2.'9 away), a smaller PA of 30° ± 9° (Fourier method), and a greater ellipticity of 0.36 (tensor method). This ellipticity is greater than 90% of the clusters inspected by Rhee et al. (1991) but is somewhat artificial because of the selection criteria. It is interesting that Bird et al. (1992) divided these inner galaxies into two clumps (noticeable in the upper left square of Fig. 7) by applying a two-dimensional spatial substructure test. Running the δ-test on this small subsample gave a Δ *less* than 99% of the simulations indicating no dynamical difference between the two components. The innermost population of our sampled galaxies thus appears very elongated and free of substructure.

Our purpose in showing the results for the inner part of the cluster is the interesting alignment in PA with the optical, X-ray and radio data. Bertola & Perola (1973) first noted the agreement between the position angle of the line perpendicular to the jets of 3C 465 (~45°), and the cD galaxy's major axis (32°). Eilek et al. (1984) further noted the agreement with the inner X-ray contours. We measured the position angle of ellipses fit to the *Einstein* IPC X-ray image centered on the cD galaxy using ELLIPSE in STSDAS and found that the PA's are 30° ± 15° for major axes between 4′ and 6′. The preferential alignment of the central dominant galaxy with its cluster position angle has been established and shown to be a stronger effect in the most elongated clusters (e.g., van Kampen & Rhee 1990). The effect may imply that the central dominant galaxies formed early on and retained the orientation of the collapsing protocluster.

5.3. *The cD Peculiar Velocity*

Perhaps the most important result of this work is the cD peculiar motion (hereafter V_{pec}). With our $N = 126$ sample, we found that the cD has a statistically significant velocity with respect to the cluster velocity centroid, -219 ± 98 km s^{-1}. This is a radial velocity and is only a component of the true velocity. We are confident in our radial velocity for the cD, but our velocity centroid $C_{BI} = 9380$ km s^{-1} should be reevaluated for subsamples of the original $N = 126$ sample. We will now try systematic approaches to reducing the V_{pec} by eliminating velocities from the distribution.

One approach to clipping would be to assume that the cluster members are well-virialized and that velocities contributing to non-normality should be removed. As mentioned above, only one galaxy needs be removed to make the velocity distribution consistent with a Gaussian above the 10% level. The V_{pec} derived using this sample is -216 ± 97 km s^{-1}.

Another approach is to eliminate the most likely nonmembers identified by their large separations from the cluster center as well as a velocity separation from the cluster. The 10 velocity *and* spatial outliers discussed above are likely nonmembers (Figs. 5 and 9). Elimination of these galaxies results in the V_{pec} of -186 ± 91 km s^{-1}. Finally, the most conservative subsample of the cluster to compare the cD velocity to is the $N = 88$ sample of innermost galaxies (§ 5.2). Even here the cD differs by $V_{pec} = -213 \pm 100$ km s^{-1}! The significance of the previous three peculiar motions remains high at 97.4%, 95.2%, and 96.7% compared to the original 98%. These clipping approaches have not eliminated the small, apparent peculiar motion.

Finally, we have performed a clipping which supports the theory that the northeast region is contaminated with a dispersed subcluster. These galaxies are almost certainly overlapping the primary cluster; the only fair way to remove them is to exclude all galaxies above a certain declination (we used 27°6′) and right ascension (we used 23^{h}38^{m}.4). This cutoff was chosen to keep the galaxies immediately around the cD in the sample. The 10 outliers were also eliminated leaving 88 velocities (different than the "innermost" galaxies, which included much of the extension). Using this sample we find $V_{pec} = -85 \pm 91$ km s^{-1}. This is consistent with a cD stationary with respect to

the primary cluster. Moreover, the northeastern 28 galaxies has a biweight centroid 500 km s^{-1} larger than that of the remaining 88. For a relaxed cluster one expects that the cluster centroid is constant with position (within counting errors).

5.4. *Normality*

Although the $N = 126$ sample was consistent with a Gaussian above the 10% level after 3 σ clipping (§ 4.5), the distribution still showed a long, high-velocity tail. The histogram (Fig. 6) also shows slight "velocity substructure" corresponding to the outlying groups at 11,700 km s^{-1}. The removal of the 10 outliers discussed above removes this substructure and greatly improves consistency with a Gaussian distribution.

The substructure observations of a possible high velocity population to the northeast (§ 4.6) suggest that the velocity distribution may be bimodal. The DIP test for bimodality (Hartigan & Hartigan 1985) gave a small value of 0.02 for the $N = 126$ sample, consistent with a unimodal distribution. However, if the subcluster constitutes only a small fraction of the sample, the DIP statistic is not sensitive enough to detect it. When the test was applied to the subsample of 28 velocities associated with all galaxies within a box drawn around the northeast extension, the DIP statistic was still not significant. The distribution did show peaks near 9300 km s^{-1} and near 10,000 km s^{-1}, however.

The 88 galaxies remaining after eliminating the 10 outliers *and* the 28 galaxies in a box to the northeast of the cD may have the velocity distribution best representative of the cluster containing 3C 465. The velocity centroid of this distribution is 9242 ± 74 km s^{-1}, hence the low cD peculiar motion (discussed above). The velocity scale is only 688 ± 58 km s^{-1}. Finally, the normality tests show the highest consistency with a Gaussian for this distribution than all others inspected.

5.5. *Implications for Cluster Formation*

We have presented all of the available information on A2634 which is relevant to understanding the evolution of this particular cluster. We measure a small peculiar motion for the cD, an agreement between our velocity distribution and a Gaussian (except for a few high-velocity outliers), an elongated cluster core, and velocity-spatial correlations possibly due to substructure.

A scenario which may explain the available observations is one of a progressed cluster–subcluster merger. Evrard (1990) laid the groundwork for simulating the cluster gas environment throughout a subcluster merger. His paper showed that the gas oscillates for a few crossing times (10^9 yr) before becoming blended into the general cluster distribution. An elongation of gas along the direction of merger persists when the galaxies are fairly well-mixed. More recently, Roettiger, Burns, & Loken (1993) have run a high-resolution three-dimensional N-body/hydro simulation of a cluster-subcluster merger like that suspected in A2634. The subcluster in their simulation was one-eighth the mass and one-half the diameter of the primary cluster. The X-ray emission plots show the gas elongating along the direction of merger, heating along shocks, and flowing rapidly through the cluster core. This is consistent with the long, asymmetric, X-ray extension in the core of A2634 (Fig. 4). It may also explain the lack of an X-ray cooling flow profile because the large-scale motion of the gas might disrupt or prevent the flow. Moreover, the residual gas motion could also provide the ram pressure needed to shape the tails of a stationary WAT and perhaps even power the WAT. As an additional benefit, the gas turbulence resulting from the merger may aid in reaccelerating particles and extending the lifetime of the radio tails (Eilek 1979). This "sloshing gas" hypothesis is favorable for the diversity of WAT morphologies (see § 1).

We can account for the small peculiar motion of the cD using the merger idea in several ways. For instance, the cD may have been given an impulse by a passing galaxy or galaxies from the subcluster. We first investigated whether the companion galaxy, N7720A would be able to provide an impulse to the cD of the magnitude which we observe. Binney & Tremaine (1987) derive expressions for the change of velocity of a point mass due to an encounter with a smaller point mass. When the encounter is *complete* and the small body is approaching infinity on a hyperbolic orbit, the change in the velocity of the large body can be expressed in terms of two components: parallel to the original velocity vector of the small mass, V_0,

$$\Delta v_{M\parallel} = \frac{2mV_0}{M+m}\left[1 + \frac{b^2V_0^4}{G^2(M+m)^2}\right]^{-1}, \quad (4)$$

and perpendicular to the original velocity vector

$$\Delta v_{M\perp} = \frac{2mbV_0^3}{G(M+m)^2}\left[1 + \frac{b^2V_0^4}{G^2(M+m)^2}\right]^{-1}. \quad (5)$$

The value within the brackets in both equations is ≈ 1. $\Delta v_{M\parallel}$ is always in the same direction as V_0. We used $b = 8$ kpc (the impact parameter; the apparent separation of N7720A and N7720 is about 8 kpc), $V_0 = 920$ km s^{-1} (the original velocity of the small mass; we used our observed radial velocity difference of the two galaxies), $M = 10^{13}$ $M_\odot$ (the cD mass), $m = 0.1M$ (De Robertis & Yee 1990 measured N7720A to be 2.7 mag fainter than N7720 and we assume the same mass-to-light ratio for both galaxies). The cD, then, undergoes an impulse with $\Delta v_{M\parallel} = 164$ km s^{-1}, and $\Delta v_{M\perp} = 23$ km s^{-1}. The net impulse could thus be ~ 170 km s^{-1} due to passage of a galaxy moving at approximately the cluster dispersion, and is sufficient to explain the bulk of the cD peculiar motion.

There are reasons to doubt that the companion is the only cause of the peculiar motion. When the internal velocity dispersion of two galaxies is near their relative velocity (or greater) tidal effects become important; but no tidal distortions were found for N7720A by De Robertis & Yee (1990) who were attempting to confirm those claimed by Lauer (1988). Moreover, it is unlikely that the cD velocity vector would be oriented radially showing the full impulse, and that the full impulse could have been imparted when the companion is projected so close to the cD.

A more satisfactory scenario is that the impulse was caused by an encounter with a merging subcluster galaxy. The problems here are identifying the galaxy responsible, and the restriction that the true peculiar motion of the cD cannot be much greater than our radial value. It is also conceivable that the cD could have an induced oscillation in the cluster potential well due to the disturbance by the entire subcluster mass.

A completely different explanation of our peculiar motion is the contamination of our velocity distribution by the merging but dispersed subcluster so that the cluster velocity centroid is no longer the same as the original cluster's centroid. This contamination effect has been observed by Beers et al. (1991) in clusters with more pronounced substructure. The velocity centroid of the subcluster members need not be very different from that of the cD; because the biweight estimator of location is resistant to outliers, removing 5–10 velocities at 1–2 σ has more affect on the centroid than at 3 σ. Our experiments on contaminating velocity distributions suggest that if our sample

contained 10–20 velocities with a mean 1000 km s^{-1} greater than that of the actual cluster, the biweight estimate of location would be increased by $\approx$150 km s^{-1}.

The northeast extension of galaxies (Fig. 8*b*, § 4.6) works well into this dispersed subcluster scenario. It has a roughly 45° orientation suggesting a trajectory through the cluster center parallel to the X-ray extension. However, the X-ray gas extends in the opposite direction from the subcluster. The WAT morphology may then be explained as the "backsloshing" of the X-ray gas. The substructure due to these galaxies was not significant using the Dressler-Shectman test but this would be expected for a *dispersed* subcluster moving in the plane of the sky. It should be stressed that the δ test will not reveal substructure when two subclusters (of equal dispersion) are orbiting each other in the plane of the sky, or when one subcluster is exactly superposed on the other. The northeast extension probably suffers from both of these problems to some extent. As discussed in § 5.3 and 5.4, we attempted to separate the subcluster contamination by removing *all* of the galaxies in the northeast from the sample. Indeed, this eliminated the radial peculiar motion of the cD and the remaining distribution has Gaussian characteristics.

6. CONCLUSIONS

We have analyzed spectroscopic data of galaxies in the field of A2634. The cluster, defined using lenient membership criteria, has a velocity centroid of 9380 km s^{-1}. We measure a small peculiar motion of the cD velocity with respect to this centroid of -219 km s^{-1} with 97% significance. The velocity distribution is basically Gaussian, depending on the level of field contamination, with $\sigma \sim 886 \pm 74$ km s^{-1}. The Dressler-Shectman δ test and close inspection reveals that one or more groups may be contributing to the significant dynamical deviations on the east side of the cluster. There also seems to be an agreement in alignment of the cD with the elongation of the cluster as well as with the X-ray and radio morphology.

From these observations, we suggest that the best evolutionary scenario for A2634 involves a small cluster merging with a primary cluster containing a stationary, dominant cD galaxy. The merging process is sufficiently progressed that substructure does not appear significant in the galaxies, but does appear in the central extension of X-ray emitting gas. The merger may provide fuel or even ignition for the WAT radio source, 3C 465. Also, the bending of the radio tails may be a result of large-scale turbulent gas motions. The alignment of the axis of symmetry of the WAT and X-ray elongation suggest that the subcluster merged along the same line. A possible dispersed subcluster is identifiable along this line. The alignment of the cluster and the cD, however, may be due to an elongated potential prior to the merger. The velocity distribution of the proposed "primary cluster" is characterized by a centroid of 9242 km s^{-1} and a scale of 688 km s^{-1}.

Much future work is needed to check the validity of the merger scenario. In particular, the ram-pressure velocity required for bending WATs needs to be better determined. More clusters, especially those with substructure or peculiar motions for their first-ranked galaxies, need to be given a multiwavelength investigation. Statistical studies such as by Malumuth et al. (1992) are needed to find what causes CDG peculiar motions. We suggest that when apparent cD peculiar motions are detected, this may signal subcluster contamination. More N-body combined with hydrodynamic simulations of mergers are needed to illuminate the behavior of the subcluster's galaxies and gas after the merger. Is there really a time when the X-ray substructure exists but the galaxy substructure is not apparent? And is it possible for the subcluster galaxies to contain a different velocity centroid than that of the primary cluster at the time when substructure has disappeared?

Special thanks to Mike Fitzpatrick, Francisco Valdes and Jeanette Barnes at NOAO for their IRAF help; to Jim Fowler, Bob Donahue and Shaun Cooper for computing assistance; to Jean Eilek and Frazer Owen for the illuminating conversations and a VLA map; to Mike Newberry for his help with early IRAF reductions; and to our referee, Eliot Malumuth, for his useful suggestions. This work was partially supported by NSF grant AST-9012353 to J. O. B., and by a Grant-in-Aid of Research from the National Academy of Sciences, through Sigma Xi to J. P.

REFERENCES

Abell, G. 1958, ApJS, 3, 211
Batuski, D., & Burns, J. O. 1985, ApJ, 299, 5
Beers, T. C., Flynn, K., & Gebhardt, K. 1990, AJ, 100, 32 (BFG)
Beers, T. C., Forman, W., Huchra, J. P., Jones, C., & Gebhardt, K. 1991, AJ, 102, 1581
Bertola, F., & Perola, G. C. 1973, Astrophys. Lett., 14, 7
Binney, J., & Tremaine, S. D. 1987, in Galactic Dynamics, ed. J. P. Ostriker (Princeton: Princeton Univ. Press)
Bird, C. M., Beers, T. C., Stanley, M., & Vance, C. T. 1992, BAAS, 24, 812
Bothun, G. D., & Schombert, J. M. 1988, ApJ, 335, 617
Burns, J. O., Norman, M. L., & Clarke, D. A. 1991, Science, 253, 485
D'Agostino, R. B. 1986, in Goodness-of-Fit Techniques, ed. R. B. D'Agostino & M. A. Stephens (New York: Marcel Dekker), 367
Danese, L., DeZotti, G., & di Tullo, G. 1980, A&A, 82, 322
De Robertis, M. M., & Yee, H. K. C. 1990, AJ, 100, 84
Dressler, A. 1980, ApJS, 42, 565
Dressler, A., & Shectman, S. A. 1988, AJ, 95, 985
Edge, A. C., & Stewart, G. C. 1991, MNRAS, 252, 414
Eilek, J. A. 1979, ApJ, 254, 472
Eilek, J. A., Burns, J. O., O'Dea, C. P., & Owen, F. N. 1984, ApJ, 278, 37
Evrard, A. E. 1990, ApJ, 363, 349
Fitchett, M. J. 1988, in Minnesota Lectures on Clusters of Galaxies and Large Scale Structure, Vol. 5, ed. J. M. Dickey (San Francisco: ASP), 143
Gebhardt, K., & Beers, T. C. 1991, ApJ, 383, 72
Griffen, R. F. 1963, AJ, 68, 421
Hartigan, J. A., & Hartigan, P. M. 1985, Ann. Stat., 13, 70
Hill, J., & Lesser, M. P. 1986, Proc. SPIE, 627, 693
———. 1988, in Instrumentation for Ground-Based Astronomy: Present and Future, ed. Lloyd B. Robinson (New York: Springer), 233
Hill, J., Hintzen, P., Oegerle, W., Romanishin, W., Lesser, M., Eisenhamer, J., & Batuski, D. 1988, ApJ, 332, L23
Jenner, D. C. 1974, ApJ, 191, 55
Jones, T. W., & Owen, F. N. 1979, ApJ, 234, 818
Keel, W. C. 1983, ApJ, 269, 466
King, I. R. 1966, AJ, 71, 64
Lauer, T. R. 1988, ApJ, 325, 49
Lucey, J. R., Gray, P. M., Carter, D., & Terlevich, R. J. 1991, MNRAS, 248, 804
Malumuth, E. M., Kriss, G. A., Van Dyke Dixon, W., Ferguson, H. C., & Ritchie, C. 1992, AJ, 104, 495
Martinez, J., & Iglewicz, B. 1981, Biometrika, 68, 331
Matthews, T. A., Morgan, W. W., & Schmidt, M. 1964, ApJ, 140, 35
Merritt, D. 1984, ApJ, 376, 26
O'Dea, C. P., & Owen, F. N. 1985, AJ, 90, 954
O'Donoghue, A., Eilek, J., & Owen, F. N. 1992, preprint
O'Donoghue, A., Owen, F. N., & Eilek, J. 1990, ApJS, 72, 75
Oegerle, W., & Hill, J. M. 1992, AJ, in press
Pearson, E. S., & Hartly, H. O. 1962, Biometrika Tables for Statisticians, Vol. 1 (Cambridge: Cambridge Univ. Press)
Pearson, E. S., & Stephens, M. A. 1964, Biometrika, 51, 484
Quintana, H., & Lawrie, D. G. 1982, AJ, 87, 1
Rhee, G. F. R. N., van Haarlem, M. P., & Katgert, P. 1991, A&AS, 91, 513
Roettiger, K., Burns, J. O., & Loken, C. 1993, ApJ, 407, L53
Sastry, G., & Rood, H. J. 1971, ApJS, 201, 371
Scott, J. S., Robertson, J. W., & Tarenghi, M. 1977, A&A, 59, 23
Shapiro, S. S., & Wilk, M. B. 1965, Biometrika, 52, 591
Sharples, R. M., Ellis, R. S., & Gray, P. M. 1988, MNRAS, 231, 479
Teague, P. F., Carter, D., & Gray, P. M. 1990, ApJS, 72, 715
Tonry, J., & Davis, M. 1979, AJ, 84, 1511
van Albada, T. S. 1982, MNRAS, 201, 939
van Kampen, E., & Rhee, G. F. R. N. 1990, A&A, 237, 283
Yahil, A., & Vidal, N. V. 1977, ApJ, 214, 347
Zabludoff, A. I., Huchra, J. P., & Geller, M. J. 1990, ApJS, 74, 1